






# The effect of organoclay loading and matrix morphology on charge transport and dielectric breakdown in an ethylene-based polymer blend

Allison V. Shaw<sup>1,\*</sup> , Alun S. Vaughan<sup>1</sup> , and Thomas Andritsch<sup>1</sup> 

<sup>1</sup> Tony Davis High Voltage Laboratory, University of Southampton, Southampton SO17 1BJ, UK

Received: 14 February 2019

Accepted: 9 June 2019

© The Author(s) 2019

## ABSTRACT

The effect of an organoclay on the electrical properties of a polymeric host is described. The matrix was composed of a blend of high- and low-density polyethylene, to which an ethylene/(vinyl acetate) copolymer was added, to increase compatibility between the organoclay and the matrix and, thereby, improve the organoclay dispersion. The ratio between the compatibiliser and organoclay was found to be important in forming a well-dispersed system, as evidenced by thermogravimetric analysis, X-ray diffraction and scanning electron microscopy, indicating the effectiveness of the chosen compatibilisation strategy. DC conductivity was found to be determined by the precise distribution of the organoclay throughout the system; changes in morphology and phase structure of the matrix polymer resulting from changes in imposed thermal history had little effect *per se*, but varying degrees of self-assembly of the organoclay facilitated by different residence times within the quiescent melt could result in changes in overall DC conductivity of several orders of magnitude. Consequent increases in DC conductivity led to reductions in DC breakdown strength, implying failure through some avalanche or thermal process. However, a monotonic increase in observed AC breakdown strength implies that the associated underlying failure process is then very different.

## Introduction

Polyethylene (PE) is a versatile polymer that can be synthesised with many different molecular architectures. As such, different polyethylenes can exhibit widely varying properties, and consequently, this family of polymers has found numerous applications. Furthermore, the mechanical, thermal or electrical

performance of PE can be additionally modified through the addition of particulate, fibrillar or lamellar fillers, which may be macroscopic, microscopic or nanometric in size. In the case of nanometric fillers, it is widely considered that the properties of the resulting nanocomposite system are, in many circumstances, markedly influenced by interfacial interactions between the polymer and the nanofiller

Address correspondence to E-mail: avb2g12@soton.ac.uk

and, as such, are conditional on the dispersion of the filler [1–3]. However, the surfaces of many commonly used inorganic fillers are polar in nature and, consequently, are relatively incompatible with PE, such that some compatibilisation strategy is required to promote the formation of a homogeneous system [3–5].

Organoclays are anisotropic materials that combine the polar silicate elements of the clay with non-polar organic moieties that are intercalated in order to enhance interactions with surrounding media. In the case of polymers, the former may interact preferentially with polar monomers, such as vinyl acetate, while the latter may be chosen to promote compatibility with species such as ethylene. Therefore, a copolymer of ethylene and vinyl acetate (EVA), being compatible with both PE and organoclays, may be employed as a means of increasing the compatibility of PE with organoclays, such that improved dispersion of the filler results [5, 6]. It has been reported that optimal organoclay loading levels fall around 5 wt%, whereby material properties are enhanced most significantly [5]. Also, it has been shown that while the thermal history of the material affects morphology and hence electrical properties [7], such effects can be mitigated by the presence of an organoclay [8].

The interplay between organoclay loading and thermal treatment influences factors such as the organoclay dispersion, polymer nucleation and morphology, modified polymer chain dynamics, the availability of charge carriers and the extent of interfacial sites acting as charge traps [9–12]. As such, material composition and thermal history can give rise to a variety of effects and, thereby, can influence electrical properties. For example, the inclusion of an organoclay has been reported to increase the DC conductivity as a consequence of it giving rise to additional charge carriers [10, 13]. In PE-based nanocomposites containing nano-alumina, increased DC conduction has been shown to lead to reduced DC dielectric breakdown strength values, [14] and presumably, comparable relationships would be anticipated in systems including organoclays. However, it has been reported that the presence of an organoclay can lead to an increase in AC dielectric breakdown strength, when the filler is well dispersed [5, 15], and a reduction in AC dielectric breakdown strength when significant agglomeration has occurred [16]. Elsewhere, the electrical performance of samples quenched rapidly from the melt was found

to be invariant to the presence of an organoclay, which is in contrast to the increased breakdown strength seen in equivalent systems following isothermal crystallisation of the matrix polymer in the absence of the organoclay [8].

Herein, we report on the interactions between polymer morphology, organoclay loading level/dispersion and electrical properties of an organoclay-based nanocomposite. The matrix was specifically chosen to be a blend of high-density PE (HDPE) and low-density PE (LDPE), since such systems can be used to generate a wide range of different lamellar textures without changing the molecular composition of the system. To this base material, EVA was added to enhance compatibility between the polymer and the organoclay filler. Different morphologies were then produced by varying the imposed thermal history, such that the extent of liquid/liquid and liquid/solid phase could be modified in a systematic manner. Through varying the organoclay loading and sample morphologies, the capability of EVA to act as a compatibiliser was evaluated.

## Experimental

### Materials and sample preparation

In this study, the following materials were used as supplied: LDPE (LD100BW, Exxon Mobil Chemicals); HDPE (Rigidex HD5813EA, BP Chemicals); EVA containing 9 wt% vinyl acetate (Elvax 750, DuPont); a montmorillonite (MMT) organoclay containing 35–45 wt% of organic components, (682624, Sigma-Aldrich). Throughout, a constant ratio of 80 parts LDPE to 20 parts HDPE by mass was used, to which the EVA was added in order to improve compatibility with the organoclay. The ratio of PE:EVA was always 80:20. The blend of LDPE and HDPE was employed herein, as elsewhere, due to its ability to form a continuous space-filling lamellar morphology where key properties are independent of variations in nucleation density [11, 17, 18].

Using the above matrix blend, five samples were produced with organoclay loadings of 0, 1, 5, 9 and 13 wt%, using a processing methodology adapted from published work [19]. Specifically, the solution blending technique was employed to aid polymer intercalation and dispersion of the nanofiller, as supported by the literature [20]. First, the organoclay

was sonicated in xylene for 30 min before being added, with the EVA, into a rotary evaporator and heated to 140 °C. When the EVA had completely dissolved, the LDPE and HDPE were added, and after complete dissolution, the resulting mixture was stirred for a further 10 min to give a homogeneous solution containing the dispersed organoclay. After this time, the resulting mixture was put under vacuum to remove the xylene, before the product was removed and further dried under vacuum at 70 °C for 6 d.

Samples 100 µm in thickness were then produced using a hydraulic press set at 140 °C. Three different thermal profiles were used to vary the morphology/phase structure of the final specimens. First, samples were quenched directly after melt pressing, to produce materials where liquid/liquid phase separation in the melt would be minimised and where rapid crystallisation would lead to a simple morphology (designated Q). For this, the samples were removed from the press and cooled to room temperature rapidly in the air. Second, the press was allowed to cool slowly to 70 °C, with the pressure applied to the sample; this process occurred over a period of 3 h, such that, in principle, the final morphology would result from a combination of liquid/liquid phase separation in the melt and subsequent liquid/solid phase separation during slow crystallisation of the polymer (designated SC). Finally, samples were held isothermally at 140 °C in the melt for 3 h before being quenched (as above for Q), in order to combine liquid/liquid phase separation in the melt with rapid subsequent crystallisation (designated ISO). These samples will hereafter be referred to using the following nomenclature: PE/EVA/X/Y where X is the organoclay loading (either 0, 1, 5, 9 or 13 wt%) and Y is the thermal profile (either Q, SC or ISO).

### Material characterisation

Thermogravimetric analysis (TGA) was conducted in both air and nitrogen atmospheres from 30 to 900 °C at a scan rate of 10 °C/min using a PerkinElmer Pyris 1 instrument, repeated three times and averaged for each system. Low-angle X-ray diffraction (XRD) measurements were performed using a Rigaku Smartlab system with a 0.2-mm slit and a Cu K $\alpha$  source, for which  $\lambda = 1.54 \text{ \AA}$ . Data were acquired for diffraction angles from  $2\theta = 0.5$  to  $2\theta = 10^\circ$   $2\theta$  using increments of  $0.02^\circ$ .

Prior to scanning electron microscopy (SEM), samples were first fractured to expose internal surfaces and then chemically etched. The etching procedure was repeated twice under constant agitation, before the samples were decanted into a quenching solution and then washed once in deionised water and then ethanol. The etchant was composed of 1 wt% potassium permanganate in a solution of sulphuric acid, phosphoric acid and water in a 5:2:1 ratio, and the quenching solution was sulphuric acid, deionised water and hydrogen peroxide in a 2:7:2 ratio [21]. The samples were then sputter-coated with gold before being examined in the SEM (EVO LS25 by Zeiss).

### Electrical properties

DC dielectric breakdown strength was measured using a ramped voltage profile with a rate of increase of 350 V/s. The AC (50 Hz) dielectric breakdown strength was measured according to ASTM D149-97a, at a ramp rate of 500 V/s. For both cases, the samples were immersed in silicone oil while being held between two vertically opposed spherical electrodes (6.3 mm diameter). The results were analysed assuming two-parameter Weibull statistics, with 90% confidence limits, using the *Origin* software package.

Measurements of DC conductivity were performed using a Keithley Instruments test fixture, 8009, and a picoammeter, 6517B. Data were acquired at different temperatures (28, 40, 55 and 70 °C) at a constant applied voltage of 300 V, which equates to an applied field of 3 kV mm. Following a preliminary study of the time dependence of conductivity, data were acquired over 1000 s, in line with the recommendations in ASTM D257. Quoted conductivity values were derived from the average of the last ten current measurements.

### Results and discussion

Figure 1 shows a range of TGA data. Figure 1a shows typical TGA traces, with their respective derivative plots, obtained from PE/EVA/0/Q and PE/EVA/5/Q in both air and nitrogen. The mass loss occurs when the organic components of each system decompose and are removed in gaseous form. For PE/EVA/5/Q, this occurs over the same temperature range for both air and nitrogen, in contrast to the

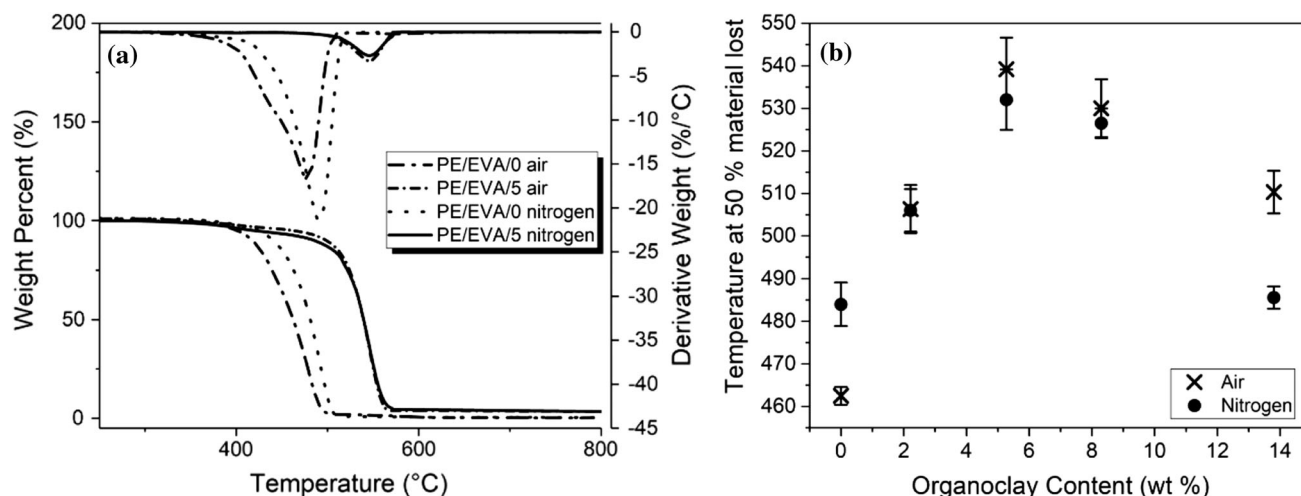


**Figure 1** TGA traces and derived data: **a** mass and derivative plots of data obtained from PE/EVA/0/Q and PE/EVA/5/Q in both air and nitrogen; **b** the achieved organoclay loadings plotted

behaviour of the unfilled PE/EVA/0/Q—this difference in behaviour is a result of the organoclay leading to a barrier effect, so increasing the temperature for thermo-oxidative degradation [22–24]. The decomposition curve of PE/EVA/5/Q also contains a shoulder that is absent in the case of PE/EVA/0/Q, which can be attributed to the initial decomposition of the quaternary ammonium salts in the organoclay [23]. The mass remaining at 800 °C in PE/EVA/5/Q represents the inorganic remnants of the clay and was used to evaluate the true organoclay loading achieved during sample preparation, the organic component of the organoclay being specified by the supplier and verified experimentally.

Figure 1b shows the effect of organoclay content on the temperature corresponding to 50% material loss. Compared to the unfilled polymer blend, it is evident that in all cases the presence of the organoclay displaces decomposition to higher temperatures, which is in line with relevant published data concerning organoclay-containing nanocomposites [24–27]. This figure also demonstrates that in all the systems other than PE/EVA/13/Q (i.e. the system containing the highest organoclay loading investigated herein), decomposition temperatures obtained in air and nitrogen are indistinguishable, within the given experimental uncertainties. Previously, such behaviour has been interpreted as providing evidence of the organoclay being well dispersed, and as such, we propose that in only the PE/EVA/13/Q system was agglomeration significant [28]. This implies the

successful use of EVA as a compatibiliser until the organoclay reached 13 wt% whereupon, presumably, the ratio of EVA to organoclay was too low to facilitate good dispersion within the PE. Finally, Fig. 1b shows that for the unfilled PE/EVA/0/Q, decomposition in nitrogen leads to a higher thermal degradation temperature than in air, whereas for PE/EVA/13/Q, decomposition in air occurs at a higher temperature than in nitrogen. We attribute this difference to different degradation mechanisms occurring when an organoclay is present, namely due to the Hofmann elimination [27].

Figure 2 compares XRD data obtained from the organoclay itself and the PE/EVA/X/Q sample set; the vertical line in this figure has been positioned to provide a marker to aid comparison of the data obtained from the different systems. First, the organoclay can be seen to be characterised by a broad peak with a maximum at  $2\theta = 3.1^\circ$ ; crystallographically, this corresponds to the interlayer periodicity within the organoclay and is, conventionally, represented as  $d_{001}$  [29, 30]. Here, this peak corresponds to a basal spacing of 2.8 nm, a result that is in line with expectations [20, 31]. Second, as anticipated, the unfilled PE/EVA/0/Q exhibits no diffraction peaks in the angular range shown, since it contains no organoclay. As such, any diffraction features seen in the following nanocomposites must be related to the state of the included organoclay which, from the data presented above, is characterised by two diffraction peaks, one which falls between  $2\theta = 2.5^\circ$  and

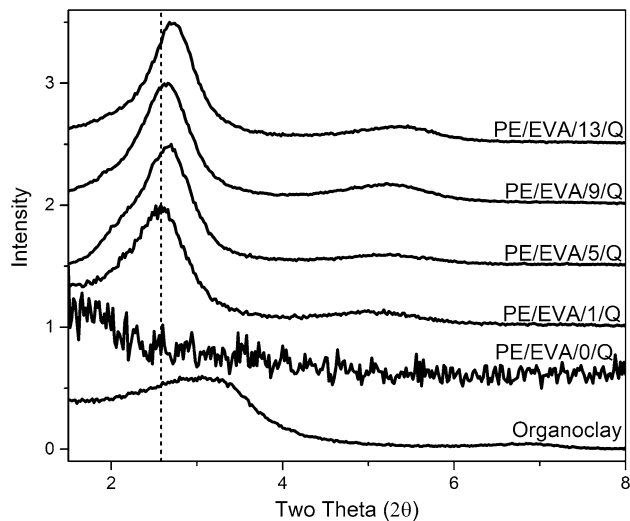


**Figure 2** XRD data derived from the PE/EVA/X/Q sample set, together with the organoclay itself. The data are offset for clarity, with a vertical line as a visual aid to assess the relative position of the peak corresponding to the interlayer distance of the organoclay.

$2\theta = 3.0^\circ$  and a smaller feature between  $2\theta = 5.0$  and  $2\theta = 6.0^\circ$ .

The former peak occurs at the lowest diffraction angle for PE/EVA/1/Q, which indicates an increase in the interlayer spacing from 2.8 nm seen in the pristine clay to 3.4 nm. Increasing the organoclay loading leads to a general reduction in the measured value of  $2\theta$  for this diffraction peak, indicating a general reduction in the interlayer spacing. For example, the peak maximum at  $2\theta = 2.8^\circ$  in the data obtained from PE/EVA/9/Q corresponds to an interlayer distance of 3.1 nm. For organoclays, the interlayer distance is determined by both the organic components of the clay and the degree of intercalation of polymer chains between the clay layers [20, 23, 32], and therefore, the above data suggest that the degree of intercalation in the systems is higher for the samples with lower organoclay loadings. Behradfar et al. [6], Mahmoudi et al. [5] and Zanetti et al. [33] all showed that intercalation in systems based upon PE and an organoclay is mediated by the presence of EVA. Elsewhere, Liang et al. [34] showed that intercalation could be enhanced by grafting polar moieties into the PE structure—maleic anhydride in this case, the key finding being that the presence and concentration of the compatibilising agent are influential in the intercalation process. Wu et al. [35] found similar results upon varying the organoclay

concentration, albeit they used entirely different polymers and offered no substantial explanation for their results. We suggest that our results can be readily interpreted in the context of the aforementioned published work. That is, at higher organoclay loadings, the ratio of polar compatibilising moieties to organoclay is reduced (the equivalent of decreasing the compatibilising agent concentration), such that the capacity for enhanced intercalation is also reduced.

The data obtained from the organoclay show an additional small and broad peak around  $2\theta = 6.8^\circ$ , within an angular range that is twice that of the principal  $d_{001}$  peak. This is consistent with data from four MMT-based organoclays published by Araújo et al. [23], and therefore, we similarly interpret it as second-order scattering from the layered structure. Although such second-order scattering features have not universally been reported for MMT-based nanocomposites [5, 6], this interpretation is consistent with published work relating to the same organoclay as used here in an HDPE–organoclay nanocomposite compatibilised by grafted maleic anhydride [20].

The variations in scattering behaviour described above are reflective of varying degrees of ordering within the systems. We take the presence of the  $d_{002}$  peak in all the data sets shown in Fig. 2 as being indicative of the presence of extensive organoclay tactoids, while the variations seen in both the  $d_{001}$  and  $d_{002}$  diffraction peaks imply variations in basal spacing and degrees of intercalation. Also, it is conceivable that some extraction of the bulky quaternary ammonium salts from the organoclay galleries may occur during solution processing; although this phenomenon has previously been reported to result from mechanical forces experienced during mixing in the melt phase [5, 6], we are not aware of reports of any comparable effects resulting from processing in solution.

The influence of material composition on sample morphology is shown in Fig. 3, which contains a representative selection of the SEM micrographs obtained across the 15 different systems considered herein. First, consider Fig. 3a–c, which illustrates the effect of increasing the organoclay content in samples slowly crystallised (PE/EVA/X/SC) and which, consequently, possess the most highly developed morphology. From Fig. 3a, it is evident that in the absence of any organoclay, crystallisation during slow cooling from the melt results in a well-

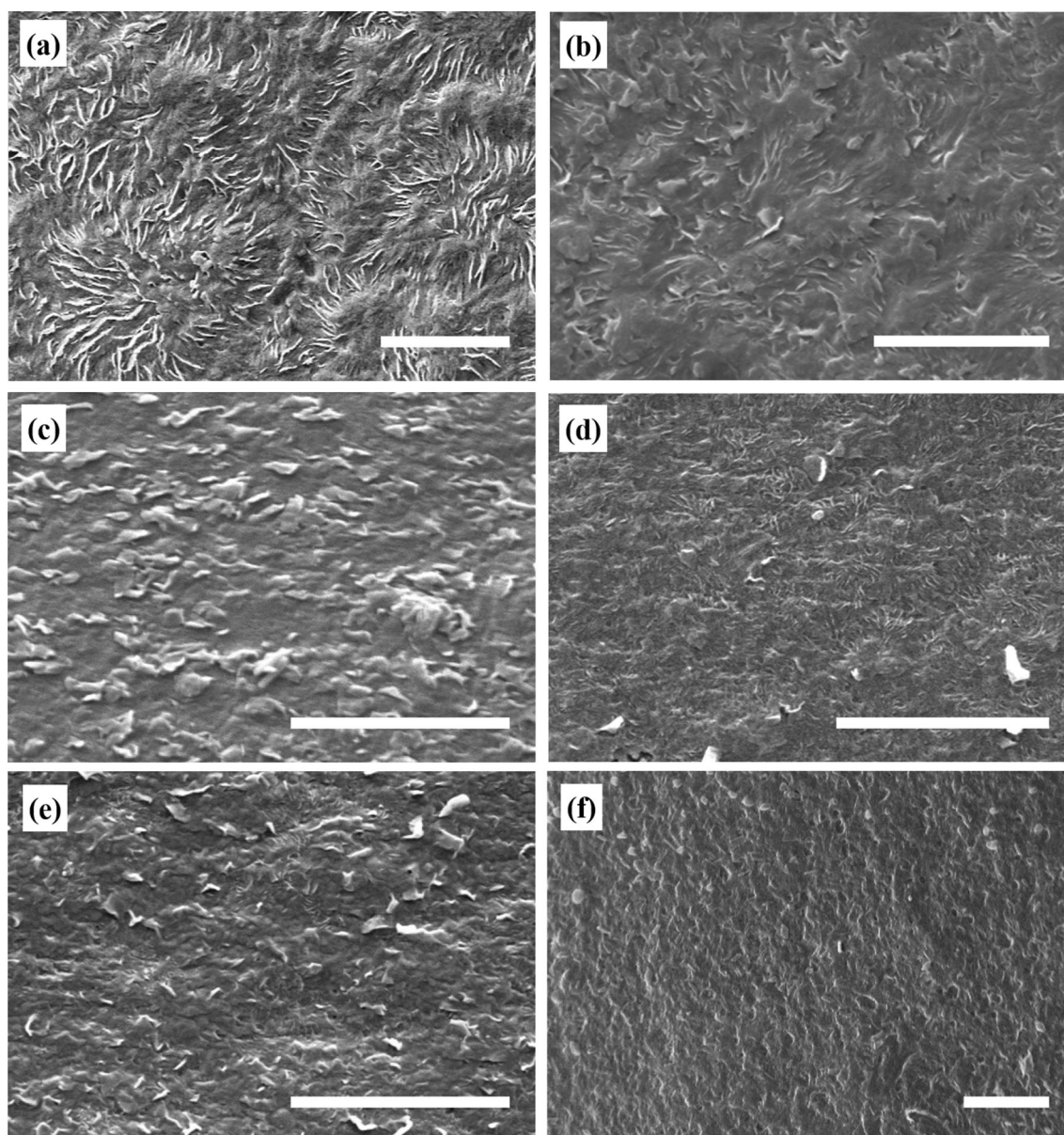


**Figure 3** SEM micrographs, with the bar representing 10  $\mu\text{m}$ , of (a) PE/EVA/0/SC, b PE/EVA/5/SC, c PE/EVA/13/SC, d PE/EVA/1/Q, e PE/EVA/9/Q and f PE/EVA/1/ISO.

developed spherulitic texture. Elsewhere [18, 36], equivalent structures have been shown to evolve in blends of HDPE and LDPE through the initial formation at relatively high temperatures of a framework of dominant lamellae composed, predominantly of the HDPE fraction of the system, followed by crystallisation of the LDPE (at a lower temperature) within the existing dominant lamellar framework. In the case of the PE/EVA blend shown here, there is no evidence of discrete EVA phases within the morphology, signifying miscibility between the EVA and the PE, such that crystallisation

of EVA occurs along with the LDPE within the HDPE-rich dominant lamellar framework. Adding the organoclay affects the observed morphology in two ways, as evidenced in Fig. 3b, c which show PE/EVA/5/SC to PE/EVA/13/SC, respectively. First, the spherulitic morphology becomes suppressed, which can be explained through both enhanced nucleation and inhibited crystal growth [8]. Second, the clay, which is barely visible in PE/EVA/5/SC, becomes much more apparent in PE/EVA/13/SC. This is consistent with the TGA and XRD results presented above.

Figure 3d, e shows samples crystallised by quenching—this strategy was employed deliberately to limit the time available for molecular fractionation and segregation processes to occur during crystallisation, such that a relatively simple morphology would develop. Comparison of the structure of PE/EVA/1/Q and PE/EVA/9/Q (Fig. 3d, e, respectively) reinforces the point made above concerning the tendency for increased organoclay agglomeration with increased loading level. Also, despite the system shown in Fig. 3d only containing 1 wt% of organoclay, no well-developed spherulitic texture is evident, an observation that is, presumably, a combination of both enhanced nucleation and rapid crystallisation, factors that inhibit the time and space available for spherulite growth, respectively. Finally, Fig. 3f shows the morphology of PE/EVA/1/ISO which, despite being held in the melt for 3 h prior to quenching, exhibits a morphology that is equivalent to that of PE/EVA/1/Q, which was quenched immediately after being formed. This supports the assertion made concerning miscibility of the EVA used here, since any significant degree of liquid/liquid phase separation would lead to the formation of discrete EVA phase regions, which is not the case.

Figure 4 compares measures of DC conductivity, as defined above, obtained at four different temperatures for the PE/EVA/X/Q sample set. Values below the sensitivity limit of the equipment were deemed unreliable and were omitted, leaving the samples

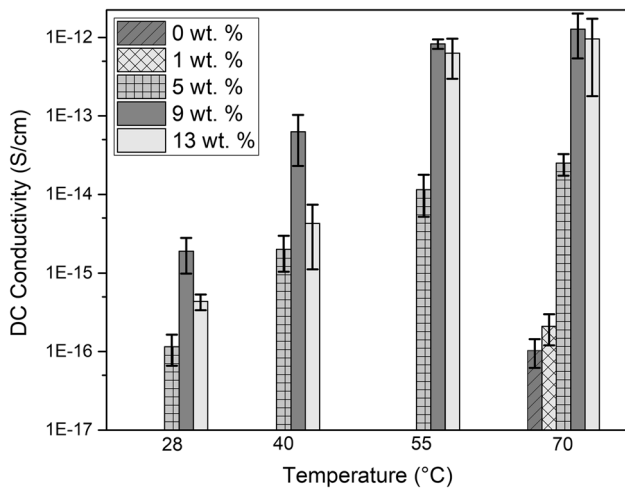


**Figure 4** DC conductivity data obtained from the PE/EVA/X/Q sample set at an applied field of 3 kV/mm at the indicated temperatures. The sensitivity limit of the measurement equipment corresponds to a conductivity of  $1 \times 10^{-17}$  S/cm and results that fell below this value have been omitted.

containing no organoclay and 1 wt% organoclay with results at only 70 °C. From these data, it is evident that conductivity increases with temperature, as would be anticipated [13, 37] and, with filler loading level from zero to 9 wt.% of organoclay. The effect of further addition of organoclay is unclear, since at 55 °C and 70 °C the systems containing 9 wt% and 13 wt% are statistically equivalent while at lower temperatures, the latter shows a decrease in conductivity compared to the former. The increased conductivity with organoclay loading may be related to a number of processes, such as the formation of neighbouring, shallow charge trapping states that can promote charge carrier mobility [38], and the introduction of additional ionic species that act as charge carriers [39]. Nevertheless, whatever the precise origin of the marked increase in conductivity with clay loading, the results presented in Fig. 4 clearly show that the presence of the clay dominates the charge transport process.

Figure 5 shows DC conductivity data taken at 70 °C in order to compare the effect of each thermal treatment. In the absence of any organoclay, the measured conductivity values all fall around  $10^{-16}$  S/cm and no clear influence of sample thermal history is evident. Similarly, the samples containing either 9 wt% or 13 wt% of the organoclay all exhibit conductivities in the range  $10^{-12}$ – $10^{-11}$  S/cm, and while their respective PE/EVA/X/ISO and PE/EVA/X/SC samples behave equivalently, the conductivity of the PE/EVA/X/Q samples at these organoclay loading levels is somewhat reduced. This is contrary to the unfilled samples, where sample thermal history does not appear to affect DC

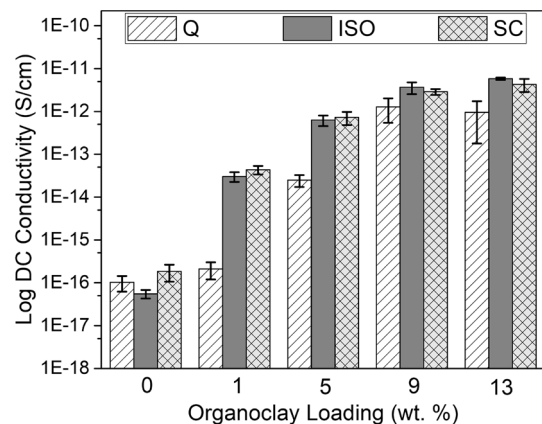


**Figure 5** Effect of specimen thermal history and organoclay loading on DC conductivity at 70 °C.

conduction processes. Differentiation between the thermal treatments is even more marked at the 1 wt% and 5 wt% organoclay loading levels with, for example, the conductivity of PE/EVA/1/Q falling two orders of magnitude below that of both PE/EVA/1/ISO and PE/EVA/1/SC.

Figures 4 and 5 taken together suggest that charge transport through an assembly of organoclay tactoids dispersed within an insulating polymer is dominated by the organoclay and, as such, we suggest that it depends upon (a) the chemical and physical characteristics of the organoclay, (b) the loading level and (c) the dispersion of the organoclay throughout the matrix. The influence of this final factor on the physical properties of composite materials has been studied in connection with numerous phenomena and material systems. For example, the formation of percolating networks within graphene-based materials has been considered extensively as a means of producing composites with increased electrical conductivity. In this context, Stankovich et al. [40] showed that reduction of graphene oxide with hydrazine could increase its electrical conductivity to the point where it is comparable to graphite, whereupon the formation of conductive networks allow charge transfer. Elsewhere, the effect of particle distribution on the thermal conductivity of polymers has attracted great interest in attempts to generate electrically insulating materials capable of effectively dissipating unwanted heat. In the case of hexagonal boron nitride (hBN), which exhibits a platelet structure, Zhou et al. [41] described a sample preparation technique that was specifically chosen to restrict dispersion throughout their HDPE matrix, thereby significantly enhancing thermal conductivity compared with equivalent systems generated by conventional melt mixing. In view of effects such as those described above, we suggest that the variations in electrical conductivity shown in Fig. 5 can be explained in terms of variations in the organoclay dispersion within the matrix polymer. That is, the long residence time in the melt that characterises both the PE/EVA/X/ISO and PE/EVA/X/SC sample sets serves to facilitate a degree of self-assembly of the organoclay within the final system. In the absence of organoclay, the resulting variations in matrix morphology have no significant effect on charge transport. At high organoclay loadings, the initially formed organoclay distributions result in vastly increased electrical conductivities such that further

modification in the structure is relatively unimportant. Only at intermediate levels—1 wt% and 5 wt%—does the arrangement of the clay tactoids evolve to a sufficient degree materially to affect the overall electrical conductivity of the system.

Figure 6 contains representative Weibull plots of DC dielectric breakdown data, obtained from the PE/EVA/0/Y sample set, from which it is evident that although the scale parameter of PE/EVA/0/ISO falls below that of the other two systems, the indicated confidence bounds of each data set largely overlap. As such, any dependence of DC dielectric breakdown behaviour on thermal history for the polymer blend considered here is small. On grounds of brevity, the DC dielectric breakdown results obtained from other material systems are summarised in terms of derived Weibull parameters and are listed in Table 1. From this, it is evident that the DC dielectric breakdown strength is adversely affected by the presence of the organoclay, and in systems containing both 5 wt% and 13 wt% of organoclay, it is the sample that was quenched that exhibits the highest DC dielectric breakdown strength. The ISO thermal treatment, in all cases, leads to the lowest breakdown strength. As such, these breakdown data are broadly consistent with the DC conductivity data described above in that increases in conductivity are generally paralleled by reductions in DC dielectric breakdown strength,

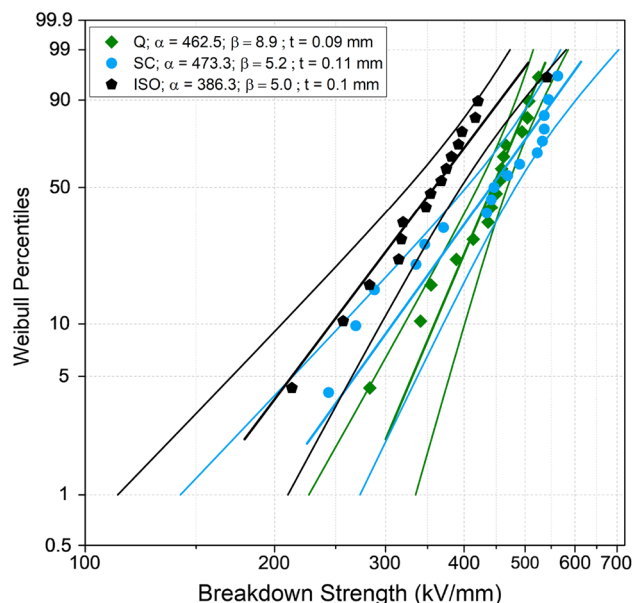


**Figure 6** Representative Weibull plots of DC dielectric breakdown data obtained from the PE/EVA/0/Y sample set.



**Table 1** Data summarising the breakdown strength values obtained from two-parameter Weibull statistics on the DC dielectric breakdown data. The error values were calculated from the upper and lower 90% limits at the 63.2% probability of failure point in the Weibull distribution

Sample, wt%	Thermal treatment	Alpha with associated error, kV/mm	Beta	Average sample thickness, mm
0	Q	463 ± 22	8.9	0.09
	ISO	386 ± 34	5.0	0.10
	SC	473 ± 38	5.2	0.11
5	Q	399 ± 13	12.6	0.10
	ISO	266 ± 20	5.8	0.10
	SC	304 ± 25	5.1	0.09
13	Q	381 ± 26	6.4	0.10
	ISO	292 ± 19	6.6	0.10
	SC	356 ± 13	11.9	0.09

suggesting that DC dielectric breakdown in these systems occurs through avalanche or thermal processes [37]. Indeed, Montanari et al. [42] reported comparable findings for PP–EVA–organoclay composites, where increases in conductivity and reductions in breakdown strength were observed and attributed to the thermal instability of the matrix to the heat generated by the current flow.

AC dielectric breakdown response of the PE/EVA/X/Q sample set is presented in the form of Weibull plots in Fig. 7. In marked contrast to the DC dielectric breakdown behaviour reported above, under AC conditions, the inclusion of the organoclay results in a monotonic *increase* in breakdown strength with organoclay loading level. It has previously been shown in a PE–EVA–organoclay composite that the AC dielectric breakdown strength increased up to a content of 5 wt%, but thereafter, further increases in organoclay loading reduced the breakdown strength, an affect ascribed to organoclay agglomeration [5]. Since our results reveal no comparable reduction in performance, it would seem that, in the material system considered here, such composition-related agglomeration effects are not sufficient to adversely impact the AC breakdown process, which is clearly very different in nature from that which operates under DC fields. Also, the above illustrates the effectiveness of our chosen EVA as a compatibiliser in that filler loadings attainable prior to agglomeration effects becoming dominant appears to be significantly higher than in the aforementioned paper. Furthermore, all of the systems considered here are characterised by increased AC dielectric breakdown strength compared with the unfilled matrix, an

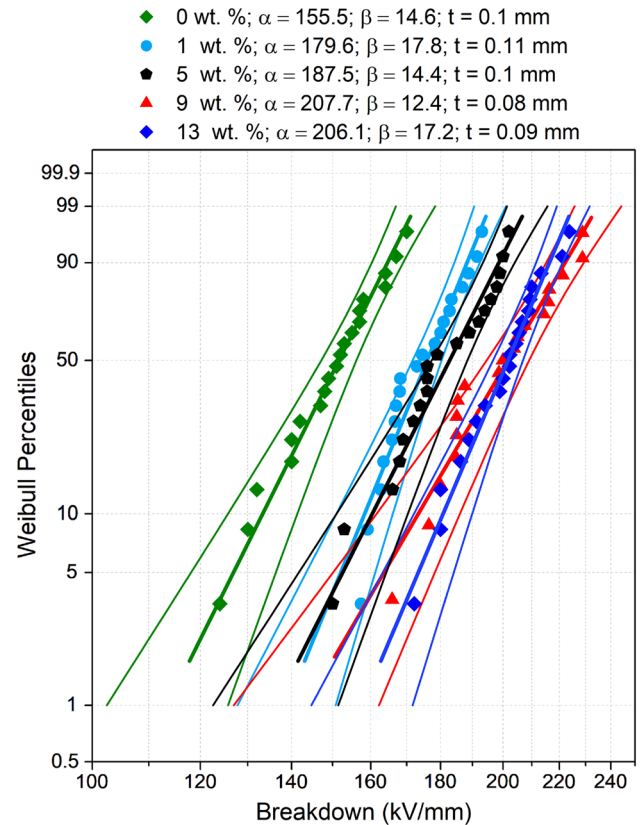


**Figure 7** AC dielectric breakdown strength data obtained from the PE/EVA/X/Q sample set. The X values with their corresponding alpha, beta and average sample thicknesses are given in the plot key.

occurrence that is generally linked to well-dispersed systems [5, 15, 43]. Therefore, these AC dielectric breakdown strength results further support our assertion that our material system achieved a good

dispersion of the organoclay and the capability of the EVA to compatibilise the system.

## Conclusions

The effect of thermal history and organoclay loading on the electrical properties of a polyethylene blend has been described, in which EVA has been used to enhance compatibility between the organoclay and the matrix and, thereby, improve the dispersion of the inorganic filler. TGA implies good dispersion of the nanofiller up to 9 wt%, as evidenced by increased decomposition temperatures and equivalent behaviour being observed in both air and nitrogen atmospheres. However, while increases in the XRD  $d_{001}$  spacing suggest a degree of polymer intercalation at lower nanoclay loading levels, as the effective ratio of organoclay to compatibiliser increases, this effect is reduced. Also, the presence of a weak  $d_{002}$  diffraction peak in all nanocomposites suggests the existence of this component as small tactoids. Real space imaging by SEM supports this, in that organoclay structures were only clearly visible at higher loading levels, while the marked morphological changes seen throughout the polymer matrix are indicative of interactions between the organoclay and the crystallising polymer that occur throughout the system. No evidence of phase separation of the EVA was seen.

Marked changes in electrical properties were seen on inclusion of the organoclay, which serves to enhance charge transport under DC applied fields. Specifically, the measured DC conductivity varied with the time the system spent in the quiescent melt, an effect we interpret in terms of variations in the spatial distribution of organoclay tactoids throughout the system. Specifically, while holding the system in the melt phase for several hours did not promote phase separation of the EVA, it did increase the DC conductivity by more than two orders of magnitude in systems containing 1 wt% of organoclay. The reduced DC breakdown strength seen in systems that exhibited increased DC conductivities is self-consistent and implies that DC breakdown occurs through an avalanche or thermal process. The monotonic increase in observed AC breakdown strength, therefore, implies that the underlying failure process is then very different.

## Acknowledgements

The authors would like to acknowledge the support of AWE plc and the support of Dr Matthew A. Brown. The authors would like to thank Dr. Suvi T. H. Virtanen from the Tony Davis High Voltage Laboratory, University of Southampton, and Dr Mark E. Light from the Department of Chemistry, University of Southampton, for their help with this work. All data supporting this study are openly available from the University of Southampton repository at <http://doi.org/10.5258/soton/d0746>.

## Compliance with ethical standards

**Conflicts of interest** The authors declare no conflict of interest.

**Open Access** This article is distributed under the terms of the Creative Commons Attribution 4.0 International License (<http://creativecommons.org/licenses/by/4.0/>), which permits unrestricted use, distribution, and reproduction in any medium, provided you give appropriate credit to the original author(s) and the source, provide a link to the Creative Commons license, and indicate if changes were made.

## References

- [1] Hoang AT, Pallon L, Liu D et al (2016) Charge transport in LDPE nanocomposites part I—experimental approach. *Polymers (Basel)* 8:1–19. <https://doi.org/10.3390/polym8030087>
- [2] Vaughan AS, Green CD, Zhang Y, Chen G (2005) Nanocomposites for high voltage applications: Effect of sample preparation on AC breakdown statistics. In: Annual report—conference on electrical insulation and dielectric phenomena, CEIDP. pp 732–735
- [3] Gopakumar TG, Lee JA, Kontopoulou M, Parent JS (2002) Influence of clay exfoliation on the physical properties of montmorillonite/polyethylene composites. *Polymer (Guildf)* 43:5483–5491. [https://doi.org/10.1016/S0032-3861\(02\)00403-2](https://doi.org/10.1016/S0032-3861(02)00403-2)
- [4] Decker JJ, Meyers KP, Paul DR et al (2015) Polyethylene-based nanocomposites containing organoclay: a new approach to enhance gas barrier via multilayer coextrusion and interdiffusion. *Polymer (Guildf)* 61:42–54. <https://doi.org/10.1016/j.polymer.2015.01.061>

- [5] Mahmoudi J, Eesaee M, Vakilian M (2013) Electrical and Mechanical Characterization of High-density Polyethylene/Ethylene Vinyl Acetate/Organoclay Nanocomposite. *IEEE Trans Dielectr Electr Insul* 20:1772–1779. <https://doi.org/10.1109/TDEI.2013.6633708>
- [6] Behradfar A, Shojaei A, Sheikh N (2010) Rheological and mechanical characteristics of low density polyethylene/ethylene-vinyl acetate/organoclay nanocomposites. *Polym Eng Sci* 50:1315–1325. <https://doi.org/10.1002/pen.21660>
- [7] Hosier IL, Vaughan AS, Swingler SG (2000) On the effects of morphology and molecular composition on the electrical strength of polyethylene blends. *J Polym Sci, Part B: Polym Phys* 38:2309–2322. [https://doi.org/10.1002/1099-0488\(2000901\)38:173.3.CO;2-Z](https://doi.org/10.1002/1099-0488(2000901)38:173.3.CO;2-Z)
- [8] Vaughan AS, Swingler SG, Zhang Y (2005) Polyethylene nanodielectrics: the influence of nanoclays on structure formation and dielectric breakdown. *IEEE Trans Japan* 126:1057–1063
- [9] Lau KY, Vaughan AS, Chen G et al (2013) Absorption current behaviour of polyethylene/silica nanocomposites. *J Phys Conf Ser* 472:012003
- [10] Tanaka T (2005) Dielectric nanocomposites with insulating properties. *IEEE Trans Dielectr Electr Insul* 12:914–928. <https://doi.org/10.1109/TDEI.2005.1522186>
- [11] Kolesov S (1980) The influence of morphology on the electric strength of polymer insulation. *IEEE Trans Electr Insul* 15:382–388. <https://doi.org/10.1109/TEI.1980.298330>
- [12] Roy M, Nelson JK, Maccrone RK et al (2005) Polymer nanocomposite dielectrics—the role of the interface. *Dielectr Electr Insul IEEE Trans* 12:629–643. <https://doi.org/10.1109/tdei.2005.1511089>
- [13] Mazzanti G, Marzinotto M (2013) Extruded cables for high-voltage direct current transmission. Institute of Electrical and Electronics Engineers, Hoboken
- [14] Jaeverberg N, Venkatesulu B, Edin H, Hillborg H (2014) Prebreakdown current and DC breakdown strength of alumina-filled poly(ethylene-co-butyl acrylate) nanocomposites: part II—Prebreakdown currents. *IEEE Trans Dielectr Electr Insul* 21:2135–2145. <https://doi.org/10.1109/TDEI.2014.003857>
- [15] Green CD, Vaughan AS, Mitchell GR, Liu T (2008) Structure property relationships in polyethylene/montmorillonite nanodielectrics. *IEEE Trans Dielectr Electr Insul* 15:134–143. <https://doi.org/10.1109/T-DEI.2008.4446744>
- [16] Brandstetter SS, Drummy LF, Horwath JC, et al (2008) Breakdown voltage of thermoplastics with clay nanometer-sized fillers. In: Proceedings of the 2008 IEEE international power modulators and high voltage conference, PMHVC, pp 287–290
- [17] Greenway GR, Vaughan AS, Moody SM (1999) Morphology and the electro-mechanical breakdown model in polyethylene. In: 1999 conference on electrical insulation and dielectric phenomena, pp 666–669
- [18] Hosier IL, Vaughan AS, Swingler SG (1997) Structure – property relationships in polyethylene blends: the effect of morphology on electrical breakdown strength. *J Mater Sci* 2:4523–4531. <https://doi.org/10.1023/A:1018617200285>
- [19] Lau KY, Vaughan AS, Chen G, Hosier IL (2012) Polyethylene nanodielectrics: the effect of nanosilica and its surface treatment on electrical breakdown strength. In: Annual report—conference on electrical insulation and dielectric phenomena, CEIDP, pp 21–24
- [20] Filippi S, Marazzato C, Magagnini P et al (2008) Structure and morphology of HDPE-g-MA/organoclay nanocomposites: effects of the preparation procedures. *Eur Polym J* 44:987–1002. <https://doi.org/10.1016/j.eurpolymj.2008.01.011>
- [21] Shahin MM, Olley RH, Blissett MJ (1999) Refinement of etching techniques to reveal lamellar profiles in polyethylene banded spherulites. *J Polym Sci Part B: Polym Phys* 37:2279–2286. [https://doi.org/10.1002/\(SICI\)1099-0488\(19990815\)37:16%3c2279:AID-POLB30%3e3.0.CO;2-L](https://doi.org/10.1002/(SICI)1099-0488(19990815)37:16%3c2279:AID-POLB30%3e3.0.CO;2-L)
- [22] Bellucci F, Camino G, Frache A et al (2013) Effect of organoclay impurities on mechanical properties of EVA-layered silicate nanocomposites. *E-Polymers*. <https://doi.org/10.1515/epoly.2006.6.1.185>
- [23] Araújo EM, Barbosa R, Morais CRS et al (2007) Effects of organoclays on the thermal processing of PE/clay nanocomposites. *J Therm Anal Calorim* 90:841–848. <https://doi.org/10.1007/s10973-006-7504-7>
- [24] Zanetti M, Bracco P, Costa L (2004) Thermal degradation behaviour of PE/clay nanocomposites. *Polym Degrad Stab* 85:657–665. <https://doi.org/10.1016/j.polyimdegradstab.2004.03.005>
- [25] Kumar S, Jog JP, Natarajan U (2003) Preparation and characterization of poly(methyl methacrylate)–clay nanocomposites via melt intercalation: the effect of organoclay on the structure and thermal properties. *J Appl Polym Sci* 89:1186–1194. <https://doi.org/10.1002/app.12050>
- [26] Fu X, Qutubuddin S (2001) Polymer–clay nanocomposites: exfoliation of organophilic montmorillonite nanolayers in polystyrene. *Polymer (Guildf)* 42:807–813. [https://doi.org/10.1016/S0032-3861\(00\)00385-2](https://doi.org/10.1016/S0032-3861(00)00385-2)
- [27] Zhao C, Qin H, Gong F et al (2005) Mechanical, thermal and flammability properties of polyethylene/clay nanocomposites. *Polym Degrad Stab* 87:183–189. <https://doi.org/10.1016/j.polyimdegradstab.2004.08.005>
- [28] Costache MC, Jiang DD, Wilkie CA (2005) Thermal degradation of ethylene-vinyl acetate copolymer

- nanocomposites. *Polymer (Guildf)* 46:6947–6958. <https://doi.org/10.1016/j.polymer.2005.05.084>
- [29] Elban WL, Howarter JA, Richardson MC et al (2012) Influence of solvent washing on interlayer structure of alkylammonium montmorillonites. *Appl Clay Sci* 61:29–36. <https://doi.org/10.1016/j.clay.2012.03.001>
- [30] Lan T, Kaviratna PD, Pinnavaia TJ (1995) Mechanism of clay tactoid exfoliation in epoxy-clay nanocomposites. *Chem Mater* 7:2144–2150. <https://doi.org/10.1021/cm00059a023>
- [31] Borah JS, Karak N, Chaki TK (2011) Effect of organoclay platelets on morphology and properties of LLDPE/EMA blends. *Mater Sci Eng, A* 528:2820–2830. <https://doi.org/10.1016/j.msea.2010.12.067>
- [32] Lu HD, Hu Y, Kong QH et al (2004) Influence of gamma irradiation on high density polyethylene/ethylene-vinyl acetate/clay nanocomposites. *Polym Adv Technol* 15:601–605. <https://doi.org/10.1002/pat.518>
- [33] Zanetti M, Costa L (2004) Preparation and combustion behaviour of polymer/layered silicate nanocomposites based upon PE and EVA. *Polymer (Guildf)* 45:4367–4373. <https://doi.org/10.1016/j.polymer.2004.04.043>
- [34] Liang G, Xu J, Bao S, Xu W (2004) Polyethylene/maleic anhydride grafted polyethylene/organic-montmorillonite nanocomposites. I. Preparation, microstructure, and mechanical properties. *J Appl Polym Sci* 91:3974–3980. <https://doi.org/10.1002/app.13612>
- [35] Wu T, Yuan D, Qiu F et al (2017) Polypropylene/polystyrene/clay blends prepared by an innovative eccentric rotor extruder based on continuous elongational flow: analysis of morphology, rheology property, and crystallization behavior. *Polym Test* 63:73–83. <https://doi.org/10.1016/j.polymertesting.2017.07.012>
- [36] Green CD, Vaughan AS, Stevens G et al (2013) Recyclable power cable comprising a blend of slow-crystallized polyethylenes. *IEEE Trans Dielectr Electr Insul* 20:1–9. <https://doi.org/10.1109/TDEI.2013.6451335>
- [37] Dissado LA, Fothergill JC (1992) *Electrical degradation and breakdown in polymers*, 1st edn. The Institution of Engineering and Technology, London
- [38] Mecheri Y, Boukezzi L, Boubakeur A, Lallouani M (2000) Dielectric and mechanical behavior of cross-linked polyethylene under thermal aging. In: 2000 Annual report conference on electrical insulation and dielectric phenomena (Cat. No.00CH37132), pp 560–563
- [39] Montanari GC, Palmieri F, Testa L et al (2006) Polarization processes of nanocomposite silicate-EVA and PP materials. *IEEJ Trans Fundam Mater* 126:1090–1096
- [40] Stankovich S, Dikin DA, Piner RD et al (2007) Synthesis of graphene-based nanosheets via chemical reduction of exfoliated graphite oxide. *Carbon N Y* 45:1558–1565. <https://doi.org/10.1016/j.carbon.2007.02.034>
- [41] Zhou W, Qi S, An Q et al (2007) Thermal conductivity of boron nitride reinforced polyethylene composites. *Mater Res Bull* 42:1863–1873. <https://doi.org/10.1016/j.materresbull.2006.11.047>
- [42] Montanari GC, Fabiani D, Palmieri F et al (2004) Modification of electrical properties and performance of EVA and PP insulation through nanostructure by organophilic silicates. *IEEE Trans Dielectr Electr Insul* 11:754–762. <https://doi.org/10.1109/TDEI.2004.1349780>
- [43] Roy M, Nelson JK, MacCrone RK, Schadler LS (2007) Candidate mechanisms controlling the electrical characteristics of silica/XLPE nanodielectrics. *J Mater Sci* 42:3789–3799. <https://doi.org/10.1007/s10853-006-0413-0>

**Publisher's Note** Springer Nature remains neutral with regard to jurisdictional claims in published maps and institutional affiliations.